Supplement of Atmos. Chem. Phys., 23, 10713–10730, 2023
https://doi.org/10.5194/acp-23-10713-2023-supplement

Atmospheric Chemistry and Physics
Open Access

Supplement of

Substantially positive contributions of new particle formation to cloud condensation nuclei under low supersaturation in China based on numerical model improvements

Chupeng Zhang et al.

Correspondence to: Yang Gao (yanggao@ouc.edu.cn) and Yuhang Wang (yuhang.wang@eas.gatech.edu)

Section S1. Model evaluations of aerosol components and gaseous pollutants

Model evaluations are conducted including $PM_{2.5}$ compositions (Fig. S1) and criteria air pollutants (Fig. S2). Observed $PM_{2.5}$ compositions include SO_4^{2-}, NO_3^-, NH_4^+, OM, and criteria air pollutants include particulate matters ($PM_{2.5}$ and PM_{10}) and gaseous pollutants (O_3, SO_2, CO, and NO_2), available at a near real-time air pollutant database (Tracking Air Pollution in China, http://tapdata.org.cn). The megacity of Beijing and a coastal city of Qingdao are selected in the evaluation, showing relatively low biases for most of the species.

Section S2. Discussion of particle number concentrations based on multiple nucleation schemes

We evaluate the performance of WRF-Chem, with updated parameterization of the particle formation and growth processes, in reproducing the observed particle number concentrations over a few other sites in the North China Plain, including one site over urban Beijing and the other one over the rural area of Gucheng (see methods in the manuscript). In February 2017, there are 10 and 5 NPF events occurred in Beijing and Gucheng, respectively (Fig. S5). The model evaluation based on these two sites in general supports the findings over the site of Qingdao. Specifically, the simulations using activation-type nucleation mechanism with the mass accommodation coefficient of sulfuric acid at 0.1 (Fig. S6 and Table S1), the same as Base in section 3.2.1, substantially overestimates the number concentration of particles in 10–40 nm. The mean fractional biases of $CN_{10–40}$ in Beijing and Gucheng are 81% and 62% respectively, which is strongly reduced to 23% and 11% by increasing the mass accommodation coefficient of sulfuric acid to 0.65 (see Section 3.2.1 of the manuscript for details).

For the larger particles (40–100 nm) which are greatly affected by the condensation process, the relevant parameters are adjusted. For instance, the modified processes include the amount of nitrate condensation in particles below 40 nm, the emission phase of primary organic aerosol (section 3.2.2 of the manuscript), and the

yield of SI-SOA (named Low_Yield, see section 3.3 of the manuscript for details). For activation-type nucleation mechanism, the mean fractional bias is reduced from 103% to 59% in Beijing, 50% to -5% in Gucheng, with correlation coefficient increasing from 0 to 0.49 and 0.46 (Fig. S7 and Table S2).

To further verify the robustness of the model improvement in reproducing the observations, we select another empirical scheme, e.g., kinetics, nucleation for evaluation. The repeated analysis for the smaller particle number concentrations ($CN_{10–40}$) indicates comparable performance between kinetics and activation schemes (Fig. S8), both showing improvement when the mass accommodation coefficient is increased from 0.1 to 0.65. Considering that the mass accommodation coefficient is suggested to reach one in some studies (Stolzenburg et al., 2020), we therefore conduct another simulation under the kinetics nucleation scheme by increasing the mass accommodation coefficient to 1.0 (purple lines in Fig. S8), yielding comparable performance but with negative mean fractional bias contrasting to the positive one based on mass accommodation coefficient of 0.65 (green lines in Fig. S8; Table S1). For the large particle number concentrations ($CN_{40–100}$), the adjusted mass accommodation coefficient (1.0) together with low yield of SI-SOA at kinetics scheme shows similar improvements as activation (Fig. S9 and Table S2).

Following the empirical nucleation scheme, we then conduct a classical nucleation mechanism to take both chemical species and meteorological conditions directly into account (Sihto et al., 2006). For instance, we select a commonly used H_2SO_4-H_2O-NH_3 ternary homogeneous nucleation which is highly dependent on temperature and relative humidity (Napari et al., 2002). The number concentrations at 10–40 nm are much higher (Fig. S10 and Table S3), at either low or high mass accommodation coefficient, compared to observations and the empirical schemes abovementioned, and the diminished effect during the adjustment of mass accommodation coefficient is likely a result of NH_3.

Contrasting to the scheme of H_2SO_4-H_2O-NH_3, the formation of sulfuric acid (SA)-dimethylamine (DMA)-water clusters has been found to be important sources of

new particle formation in megacities over China (Yao et al., 2018). Bergman et al. (2015) applied amine-enhanced nucleation parameterization to an aerosol climate model to estimate the effect of amine on new particle formation on a global scale, indicating that high nucleation rates are confined to regions close to the amine source due to the short lifetime of amines. Because of the short life of amines, the emission of amines remains to be highly uncertain and deserves further investigation (Chang et al., 2021). By comparing this classical nucleation scheme with the empirical one (e.g., kinetics), the spatial distibutions of particle formation rate between these two types of nucleation schemes are largely consistent.

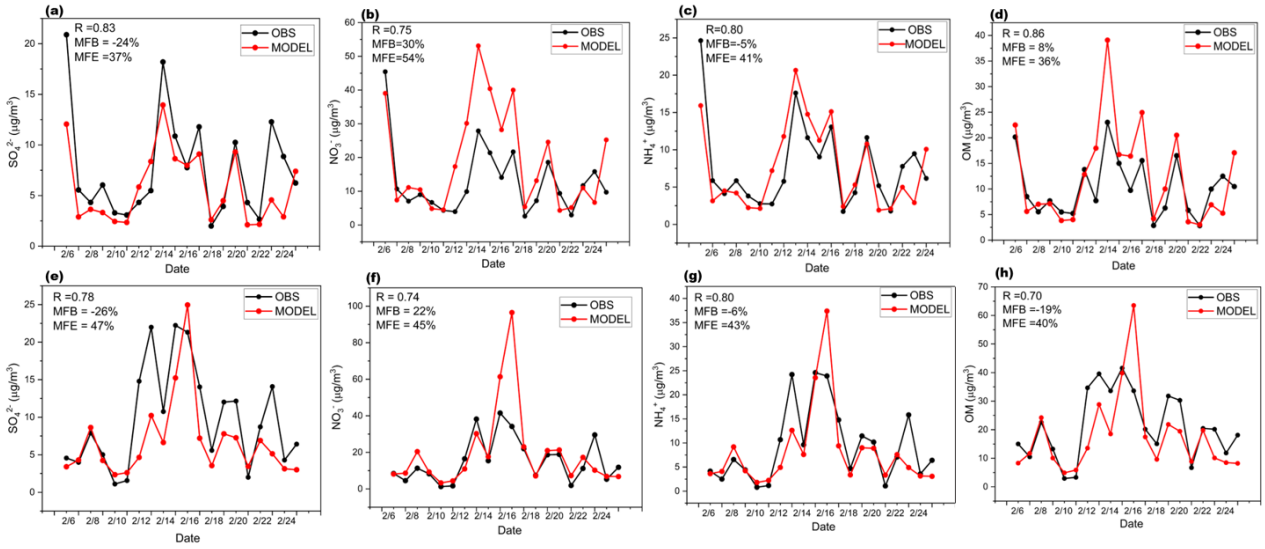

Fig. S1. The comparison between model simulations (red lines) and observations (black lines) from February 5 to February 24, 2017. Shown are results of the average daily concentration of the four main components of $PM_{2.5}$ (SO_4^{2-}, NO_3^-, NH_4^+, OM) in Qingdao (top) and Beijing (bottom). Statistical indicators including mean fractional bias (MFB), mean fractional error (MFE) and correlation coefficient (R) are also displayed in the upper left corner of each panel.

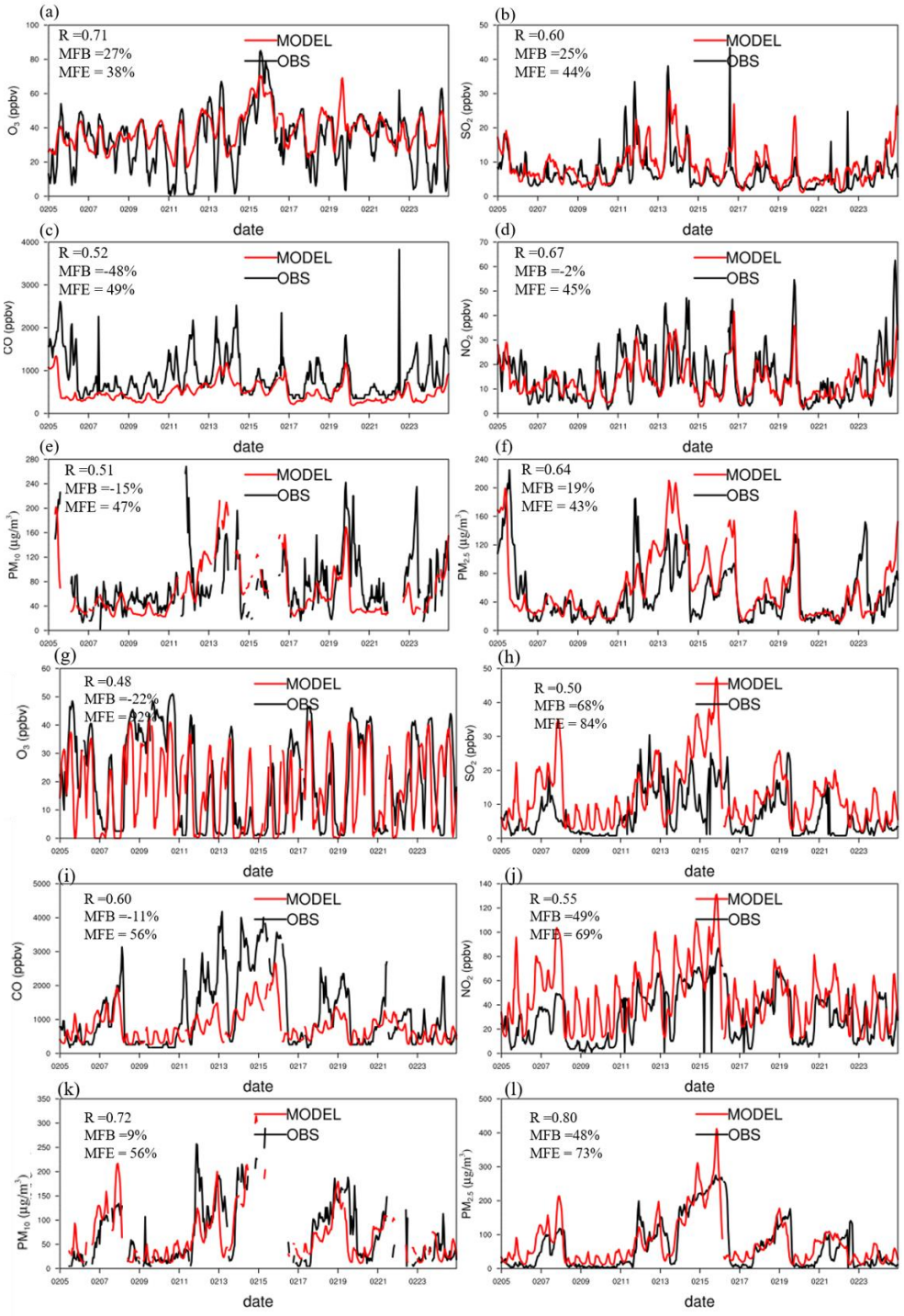

Fig. S2. The comparison between model simulations and observations from February 5 to February 24, 2017. Shown are results of concentrations of air pollutants (O_3, SO_2, CO NO_2, PM_{10} and $PM_{2.5}$) in Qingdao (Fig. S2a−f) and Beijing (Fig. S2g−l). Statistical indicators including mean fractional bias (MFB), mean fractional error (MFE) and correlation coefficient (R) are also displayed in the upper left corner of each panel.

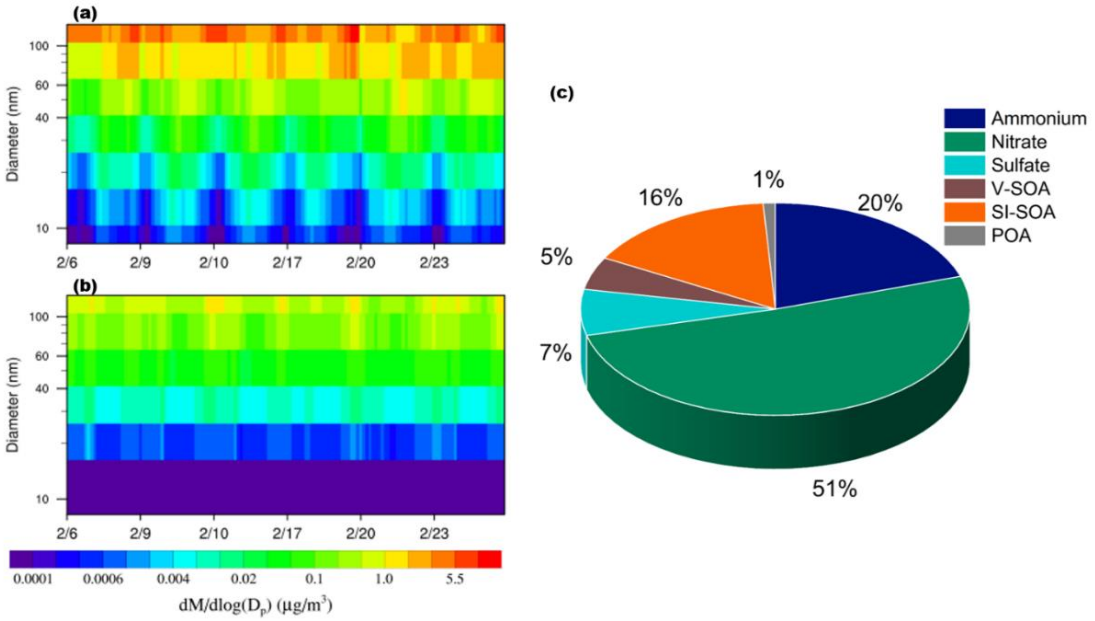

Fig. S3. Modeled size resolved mass concentration of primary organic aerosol (POA) in each size bin simulated by (a) MAC and (b) PEP, and the mass fractions of the major chemicals in the 10–40 nm particles obtained from the PEP simulations.

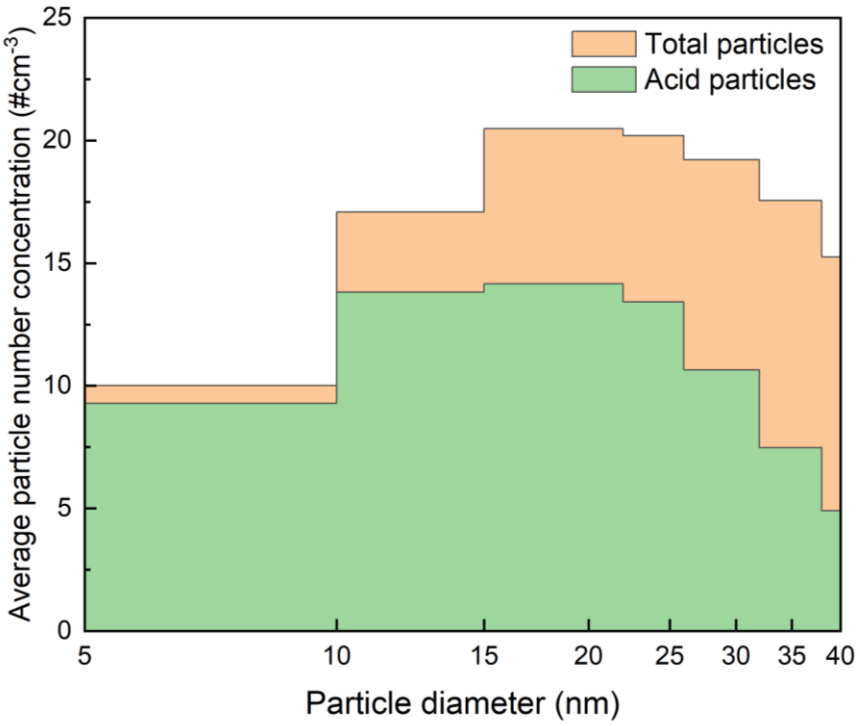

Fig. S4. Average particle number concentration of total environmental particles (marked in orange) and acid particles (marked in green) as a function of particle size in Hong Kong from 22 December 2010 to 15 January 2011 as reported by Wang et al. (2014).

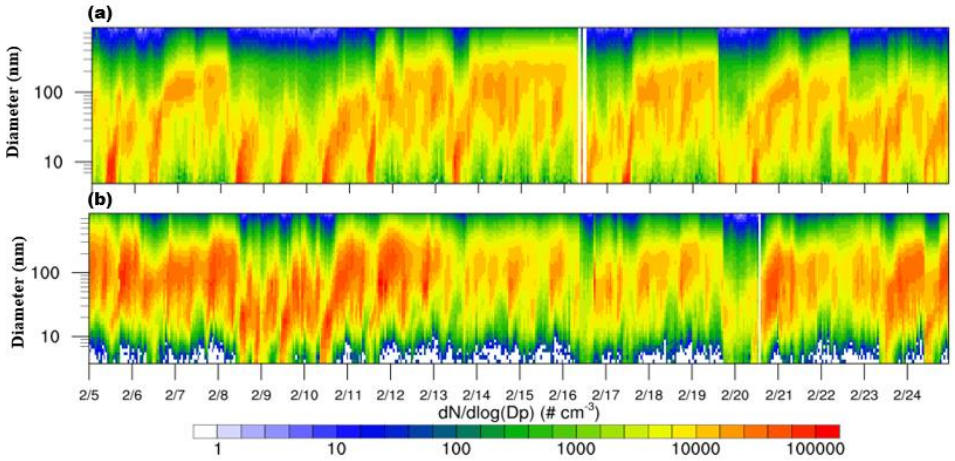

Fig. S5. Observed particle number concentration distribution in the size range of 10–800 nm in (a) Beijing and (b) Gucheng on February 5-24, 2017. All times are local times (LT).

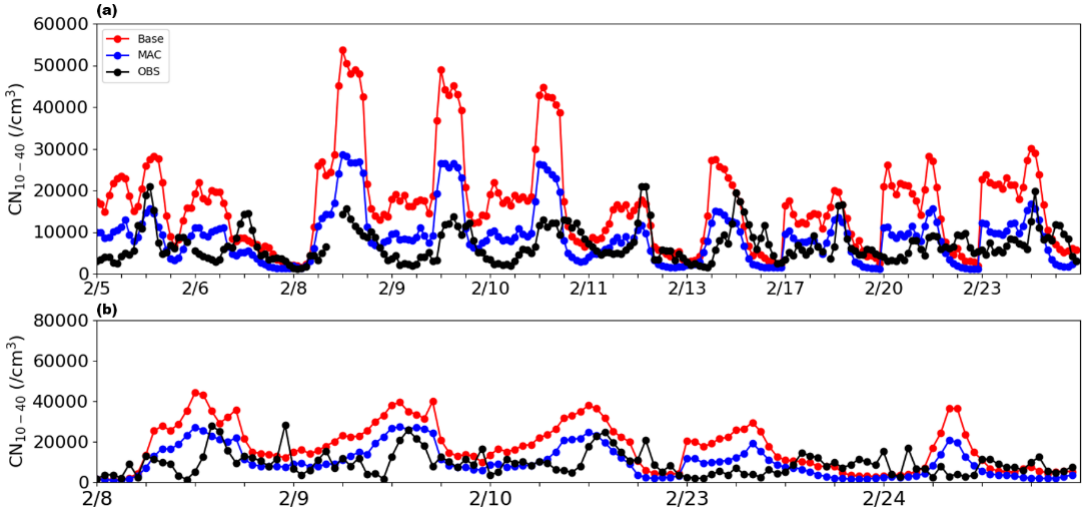

Fig. S6. The time series of $CN_{10–40}$ on NPF days in (a) Beijing and (b) Gucheng on February 5-24, where red and blue represent Base and MAC simulation results respectively. All times are local times (LT).

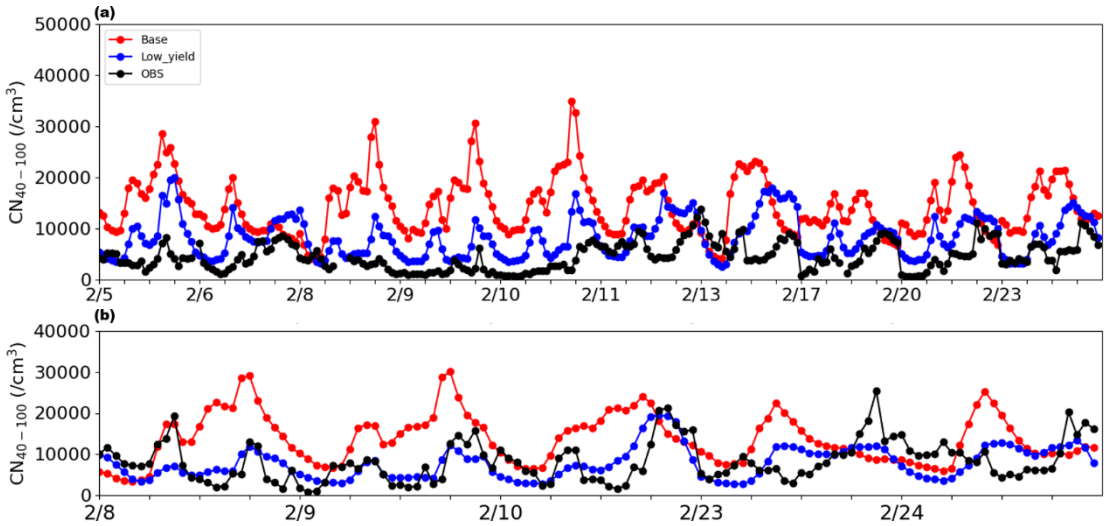

Fig. S7. The time series of $CN_{40–100}$ on NPF days in (a) Beijing and (b) Gucheng on February 5-24, where red and blue represent Base and Low_Yield simulation results respectively. All times are local times (LT).

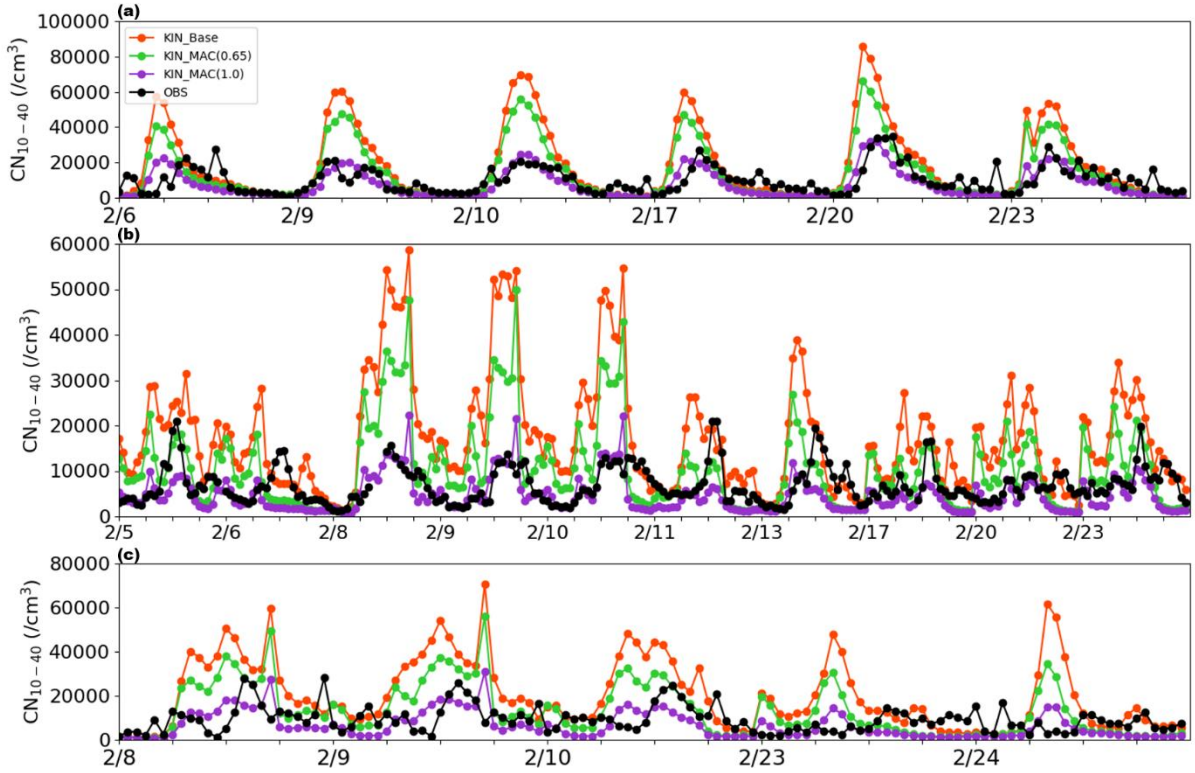

Fig. S8. The time series of $CN_{10–40}$ on NPF days in (a) Qingdao, (b) Beijing and (c) Gucheng on February 5-24 simulated by Base (marked in orange) and MAC (green and purple lines corresponding to sulfuric acid mass coefficient of 0.65 and 1, respectively). All times are local times (LT).

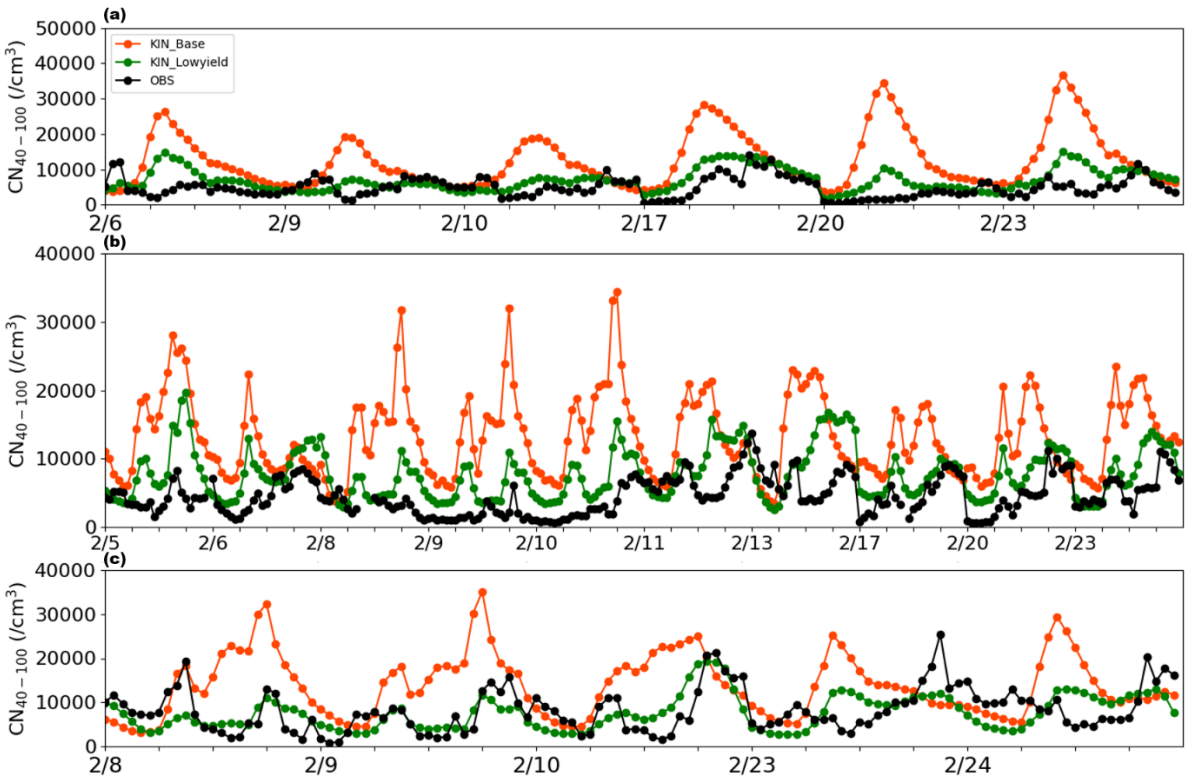

Fig. S9. The time series of $CN_{40–100}$ on NPF days in (a) Qingdao, (b) Beijing and (c) Gucheng on February 5-24 simulated by Base (marked in orange) and Low_Yield (marked in dark green) using kinetics nucleation scheme (KIN) as well as from observations (OBS) (marked in black). All times are local times (LT).

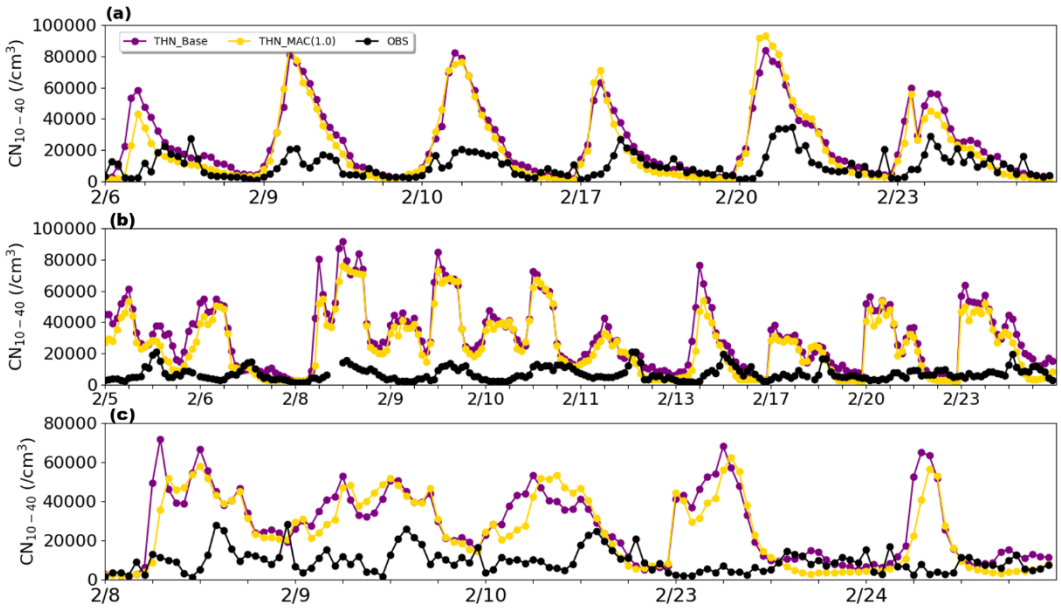

Fig. S10. The time series of $CN_{10–40}$ on NPF days in (a) Qingdao, (b) Beijing and (c) Gucheng on February 5-24 simulated by Base (marked in purple) and MAC (marked in yellow) using H_2SO_4-H_2O-NH_3 ternary homogeneous nucleation (THN) as well as from observations (OBS) (marked in black). All times are local times (LT).

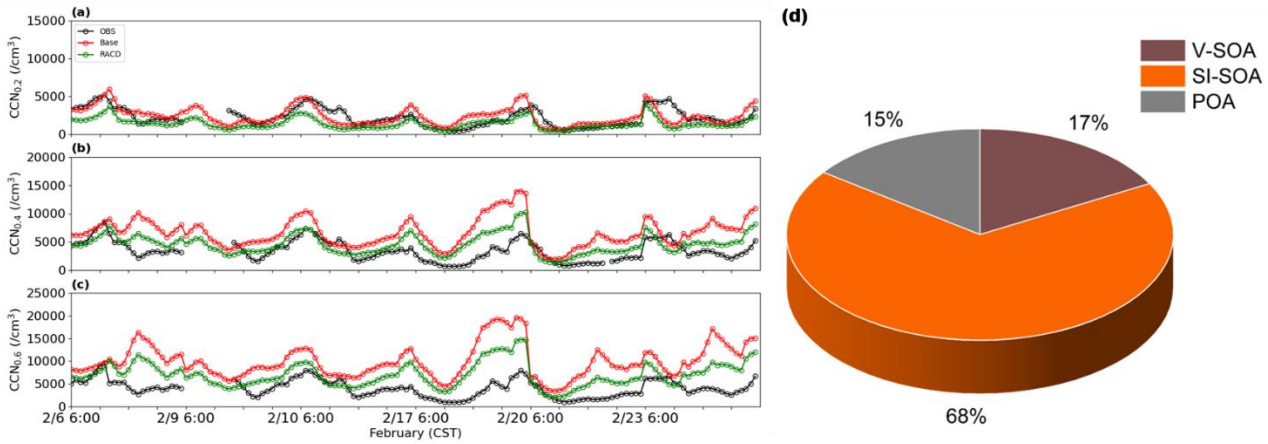

Fig. S11. The time series of (a) $CCN_{0.2\%}$, (b) $CCN_{0.4\%}$ and (c) $CCN_{0.6\%}$ on NPF days simulated Base (marked in red) and RACD (marked in green) as well as from observations (OBS) (marked in black), and (d) the proportion of different components of organic matter in 1–100 nm particles, where orange represents SI-SOA, brown represents V-SOA, and grey represents POA.

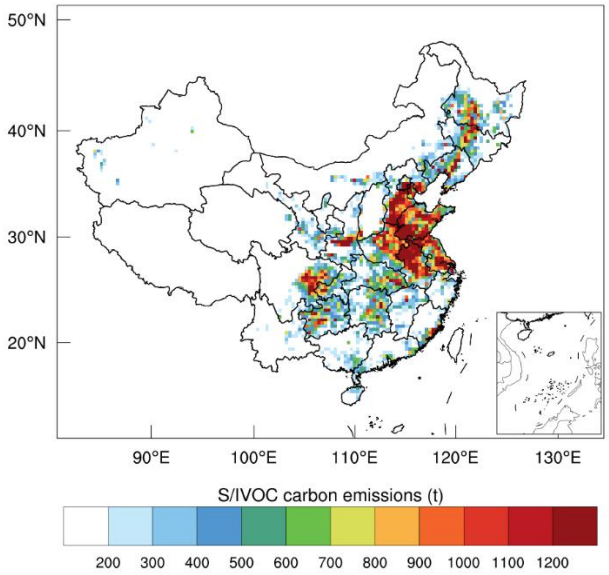

Fig. S12. Spatial distribution of total S/IVOC carbon emissions in mainland China in February 2017.

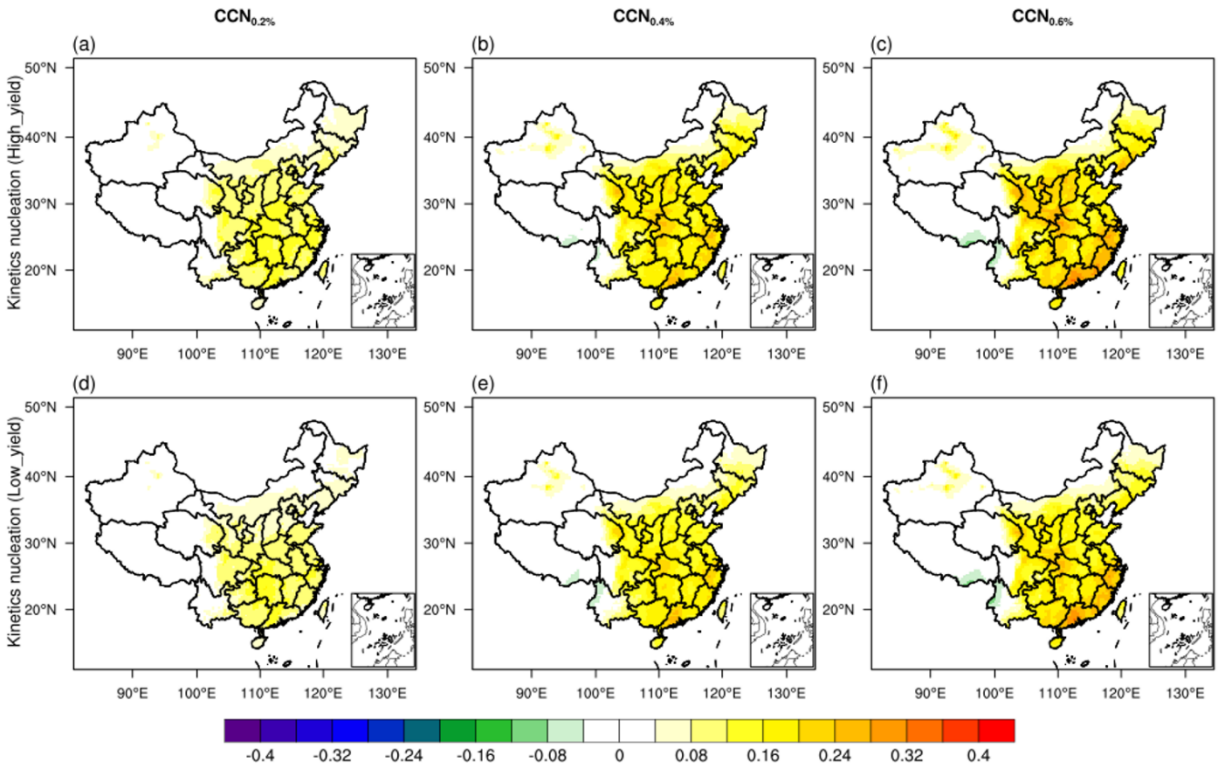

Fig. S13. Spatial distribution of contribution of nucleation to CCN calculated by the ratio of the difference between the parameterization with and without nucleation (kinetics nucleation scheme) to the parameterization with nucleation under different SI-SOA yields in China in February 2017. (a, d) is $CCN_{0.2\%}$, (b, e) is $CCN_{0.4\%}$, (c, f) is $CCN_{0.6\%}$. The upper panel and lower panel represent High_Yield and Low_Yield simulation respectively.

Table S1 The statistics of model simulation from empirical nucleation mechanism and observation data for CN_{10-40} in Qingdao, Beijing and Gucheng.

Observational sites / Simulation	Qingdao			Beijing			Gucheng		
	MFB (%)	MFE (%)	R	MFB (%)	MFE (%)	R	MFB (%)	MFE (%)	R
ACT_Base	48%	66%	0.69	81	90	0.35	62	82	0.21
ACT_ MAC(0.65)	1%	49%	0.70	23	65	0.39	11	67	0.13
KIN_Base	58%	83%	0.60	86	91	0.41	76	93	0.13
KIN_ MAC(0.65)	40%	71%	0.60	41	78	0.34	37	81	0.18
KIN_MAC(1.0)	-30%	57%	0.69	-40	61	0.41	-34	81	0.23

Table S2 The statistics of model simulation from empirical nucleation mechanism and observation data for CN_{40-100} in Qingdao, Beijing and Gucheng.

Observational sites / Simulation	Qingdao			Beijing			Gucheng		
	MFB (%)	MFE (%)	R	MFB (%)	MFE (%)	R	MFB (%)	MFE (%)	R
ACT_Base	98	102	0	103	106	0	50	72	0
ACT_Lowyield	32	53	0.42	59	65	0.47	-5	47	0.46
KIN_Base	88	94	0	97	100	0	50	74	0
KIN_Lowyield	36	52	0.39	53	60	0.49	-7	48	0.46

Table S3 The statistics of model simulation from ternary homogeneous nucleation and observation data for CN_{10-40} in Qingdao, Beijing and Gucheng.

Observational sites / Simulation	Qingdao			Beijing			Gucheng		
	MFB (%)	MFE (%)	R	MFB (%)	MFE (%)	R	MFB (%)	MFE (%)	R
THN_Base	85	93	0.68	126	128	0.10	101	108	0.05
THN_MAC(1.0)	72	93	0.52	113	122	0.12	82	95	0.21

References:

Bergman, T., Laaksonen, A., Korhonen, H., Malila, J., Dunne, E. M., Mielonen, T., Lehtinen, K. E. J., Kühn, T., Arola, A., Kokkola, H.: Geographical and diurnal features of amine-enhanced boundary layer nucleation, Journal of Geophysical Research: Atmospheres, 120, 9606-9624, doi: https://doi.org/10.1002/2015JD023181, 2015.

Chang, Y., Gao, Y., Lu, Y., Qiao, L., Kuang, Y., Cheng, K., Wu, Y., Lou, S., Jing, S., Wang, H., Huang, C.: Discovery of a Potent Source of Gaseous Amines in Urban China, Environ. Sci. Technol. Lett., 8, 725-731, doi: 10.1021/acs.estlett.1c00229, 2021.

Napari, I., Noppel, M., Vehkamäki, H., Kulmala, M.: Parametrization of ternary nucleation rates for H2SO4-NH3-H2O vapors, J. Geophys. Res. Atmos., 107, AAC 6-1-AAC 6-6, doi: https://doi.org/10.1029/2002JD002132, 2002.

Sihto, S. L., Kulmala, M., Kerminen, V. M., Dal Maso, M., Petäjä, T., Riipinen, I., Korhonen, H., Arnold, F., Janson, R., Boy, M., Laaksonen, A., Lehtinen, K. E. J.: Atmospheric sulphuric acid and aerosol formation: implications from atmospheric measurements for nucleation and early growth mechanisms, Atmos. Chem. Phys., 6, 4079-4091, doi: 10.5194/acp-6-4079-2006, 2006.

Stolzenburg, D., Simon, M., Ranjithkumar, A., Kürten, A., Lehtipalo, K., Gordon, H., Ehrhart, S., Finkenzeller, H., Pichelstorfer, L., Nieminen, T., He, X. C., Brilke, S., Xiao, M., Amorim, A., Baalbaki, R., Baccarini, A., Beck, L., Bräkling, S., Caudillo Murillo, L., Chen, D., Chu, B., Dada, L., Dias, A., Dommen, J., Duplissy, J., El Haddad, I., Fischer, L., Gonzalez Carracedo, L., Heinritzi, M., Kim, C., Koenig, T. K., Kong, W., Lamkaddam, H., Lee, C. P., Leiminger, M., Li, Z., Makhmutov, V., Manninen, H. E., Marie, G., Marten, R., Müller, T., Nie, W., Partoll, E., Petäjä, T., Pfeifer, J., Philippov, M., Rissanen, M. P., Rörup, B., Schobesberger, S., Schuchmann, S., Shen, J., Sipilä, M., Steiner, G., Stozhkov, Y., Tauber, C., Tham, Y. J., Tomé, A., Vazquez-Pufleau, M., Wagner, A. C., Wang, M., Wang, Y., Weber, S. K., Wimmer, D., Wlasits, P. J., Wu, Y., Ye, Q., Zauner-Wieczorek, M., Baltensperger, U., Carslaw, K. S., Curtius, J., Donahue, N. M., Flagan, R. C., Hansel, A., Kulmala, M., Lelieveld, J., Volkamer, R., Kirkby, J., Winkler, P. M.: Enhanced growth rate of atmospheric particles from sulfuric acid, Atmos. Chem. Phys., 20, 7359-7372, doi: 10.5194/acp-20-7359-2020, 2020.

Wang, D.-W., Guo, H., Chan, C.: Diffusion Sampler for Measurement of Acidic Ultrafine Particles in the Atmosphere, Aerosol Sci Technol, 48, doi: 10.1080/02786826.2014.978937, 2014.

Yao, L., Garmash, O., Bianchi, F., Zheng, J., Yan, C., Kontkanen, J., Junninen, H., Mazon, S., Ehn, M., Paasonen, P., Sipilä, M., Wang, M., Wang, X., Xiao, S., Chen, H., Lu, Y., Zhang, B., Wang, D., Fu, Q., Wang, L.: Atmospheric new particle formation from sulfuric acid and amines in a Chinese megacity, Science, 361, 278-281, doi: 10.1126/science.aao4839, 2018.